Internal Waves in the Vicinity of the Kuroshio Path

Ren-Chieh Lien
Applied Physics Laboratory
University of Washington
Seattle, Washington 98105
phone: (206) 685-1079 fax: (206) 543-6785 email: lien@apl.washington.edu

Award Number: N00014-04-1-0237

LONG-TERM GOALS

My long-term scientific goals are to understand the dynamics of small-scale processes and to quantify the mechanisms by which mixing occurs in the ocean and thereby help develop improved parameterizations of mixing for ocean models. Mixing within the stratified ocean is a particular focus as the complex interplay of internal waves from a variety of sources and turbulence makes this a current locus of uncertainty. A better understanding of energy sources and the dynamics of internal waves will help improve a physics-based parameterization scheme for ocean models.

OBJECTIVES

For this project, our broad focus is on inertial waves, internal tides, the internal wave continuum, and nonlinear internal waves in a complex and diverse dynamic environment (Fig. 1) where the Kuroshio interacts with the shallow and the deep topography (Tang et al., 2003), strong nonlinear internal waves and finescale inertial shear layers are observed (Rainville and Pinkel, 2004), and strong internal tides have been suggested by numerical models (Niwa and Hibiya, 2004). The primary objectives of this project are 1) to provide a geographical map and the long-term variation of internal wave energy and shear variances, 2) to quantify high-frequency nonlinear internal wave energy, and 3) to quantify the energy and shear of inertial waves along the Kuroshio path.

APPROACH

We will analyze observations taken in the vicinity of the Kuroshio path from the Luzon Strait to the southern East China Sea. Available data sets include 1) moored and bottom mounted ADCPs, and shipboard ADCP observations, 2) CTD profiles, 3) moored temperature, 4) moored current meter, and 5) echo sounder. Previous studies of these data focused primarily on sub-inertial processes. Most of available data were taken at a sampling rate of < 60 minutes, suitable for studying internal waves.

WORK COMPLETED

- A preliminary analysis of historical CTD data was performed to quantify the seasonal variations of the Kuroshio front in the Luzon Strait and along the east coast of Taiwan.
- With Dr. Jan Sen we performed a numerical model simulation to investigate the energy budget of barotropic and baroclinic tides in the Luzon Strait (Jan et al., 2008). We identified the generation and dissipation sites of baroclinic tides and quantified the energy flux, the generation rate, and the dissipation of barotropic and baroclinic tides.

RESULTS

The water mass east of the Philippines is often defined as Kuroshio water (black block in Fig. 2), and the water mass west of the Philippines is often defined as South China Sea water (red block in Fig. 2) (Chern and Wang, 1998). Within the Kuroshio along the east coast of Taiwan, both types of water have been observed (Fig. 3). It is unclear where and how these two water masses mix. Within the Luzon Strait the Kuroshio, barotropic tides, baroclinic tides, and other oceanic processes interact with submarine ridges; they are potential sources for the turbulence mixing (Fig. 2).

Averaged density fields across the Kuroshio along the east coast of Taiwan in summer and in winter were constructed using historical CTD data collected by the National Center for Ocean Research (NCOR) between 1985 and 2002 (Figs. 4 and 5). The isopycnal tilts associated with the Kuroshio and the boundary countercurrent along the east coast of Taiwan are revealed. Similar temperature and salinity fields were constructed, as well as fields of their standard deviations (not shown). We are in the process of quantifying the seasonal and geographical variations.

The spatial and temporal variations of baroclinic tides in the Luzon Strait were investigated using a three-dimensional tide mode. Luzon Strait is the primary deep passage between the Pacific Ocean and the South China Sea (Figure 6). The Kuroshio and tides are the dominant currents in the Luzon Strait. The barotropic tidal currents oscillate at amplitudes of 0.05–0.3 m s^{-1} with major axes nearly perpendicular to the two ridges in the Luzon Strait such that strong baroclinic tides are generated. The double ridges cause strong dissipation of barotropic and baroclinic tidal energy. The energy budget is summarized in Figure 6b. On average, 30 GW of baroclinic tidal energy, including all four major tidal constituents, are generated within the Luzon Strait. About 6.6 GW of baroclinic tidal energy propagates into the South China Sea, and 5.6 GW of baroclinic tidal energy propagates into the Pacific Ocean. There is a loss of 18 GW of baroclinic tidal energy within the Luzon Strait either via turbulence mixing or transformed into non-hydrostatic processes, e.g., nonlinear internal waves (NLIWs), which are not resolved by the model. Previous studies show the energy flux of NLIWs in the South China Sea is ~2 GW (Klymak et al., 2006). Assuming all the loss of baroclinic tidal energy is dissipated locally within the Luzon Strait, the average turbulence kinetic energy dissipation rate per unit mass, ε, within the Luzon Strait is ~10^{-7} W kg^{-1}, and a bulk estimate of the vertical eddy diffusivity is O(10^{-3}) m^2 s^{-1}. The inferred turbulence kinetic energy dissipation rate and vertical eddy diffusivity are a factor of 100 greater than those in a typical open ocean suggesting strong turbulence mixing induced by breaking baroclinic tides.

Details of barotropic to baroclinic tidal energy conversion and energy fluxes for four individual tidal constituents are shown in Figure 7. Among the four tidal constituents, the S2 baroclinic tide is the weakest within the Luzon Strait. About 70% of baroclinic tidal energy is generated at the east ridge, and 30% is generated at the west ridge. The semidiurnal M_2 baroclinic tide propagates into the South China Sea and the Pacific Ocean in a narrow tidal beam, ~100 km.

The energy budget and the energy fluxes of baroclinic tides forced by the combined four major tidal constituent do not show significant seasonal variation. There is strong fortnightly variation (Figure 8). The baroclinic tidal energy generation, energy fluxes, and energy dissipation rates in the spring tide are about five times those in the neap tide.

IMPACT/APPLICATION

The mass, heat, momentum, and energy transports of the Kuroshio are potentially important for modulating Asian waters. To improve our skill of modeling turbulent processes and quantifying turbulence mixing within the Kuroshio and between the Kuroshio and surrounding water, we need to identify energy sources of internal wave and turbulence mixing along the Kuroshio path. Results of the present analysis of historical data will provide the spatial and temporal distributions of internal wave energy and shear variances along the path of the Kuroshio and improve our understanding of the Kuroshio dynamics.

The numerical model results of baroclinic tides in Luzon Strait suggest strong baroclinic tidal energy generation and dissipation within the Luzon Strait. The strong turbulence mixing caused by baroclinic tides could be crucial for modifying water masses of the Kuroshio, South China Sea, and Pacific Ocean.

RELATED PROJECTS

Energy Budget of Nonlinear Internal Waves near Dongsha (N00014-05-1-0284) as a part of NLIWI DRI:

In this project, we study the dynamics and quantify the energy budget of nonlinear internal waves (NLIWs) in the South China Sea using observations taken from two intensive shipboard experiments in 2005 and 2007 and a set of nearly one year of velocity-profile measurements taken in 2006–2007 from three bottom mounted ADCPs across the continental slope east of Dongsha Plateau in the South China Sea. NLIWs in the South China Sea are generated either directly in the Luzon Strait or are transformed from internal tides that are generated in the Luzon Strait. Understanding the generation, dissipation, and propagation of internal tides within the Luzon Strait is critically important for studying the energy budget of NLIWs in the South China Sea.

REFERENCES

Chern, C.-S., J. Wang, The spreading of the South China Sea water to the east of Taiwan during summertime, *Acta Ocean.. Taiwanica*, **36**, 97-109, 1998.

Klymak, J. M., R. Pinkel, C.-T. Liu, A. K. Liu, and L. David, Prototypical solitons in the South China Sea, *Geophys. Res. Lett*., **33**, L11607, doi:10.1029/2006GL025932, 2006.

Liang, W. D., T. Y. Tang, Y. J. Yang, M. T. Ko, and W. -S. Chuang, Upper-ocean currents around Taiwan, *Deep Sea Res*., **40**, 1085-1105, 2003.

Niwa, Y. and T. Hibiya, Three-dimensional numerical simulation of the M2 internal tides in the East China Sea, *J. Geophys. Res., 109, C04027,* doi:10.1029/2003JC001923, 2004.

Rainville, L., and R. Pinkel, Observations of energetic high-wavenumber internal waves in the Kuroshio, *J. Phys. Oceanogr.,* **34**, 1495-1505, 2004.

Tang, T. Y., H. Y. Tai, and Y. J. Yang, The flow pattern north of Taiwan and the migration of the Kuroshio, *Cont. Shelf Res*., **20**, 349-371, 2003.

PUBLICATIONS

Jan, S., R.-C. Lien, and C.-H. Ting, Numerical study of baroclinic tides in Luzon Strait, *J. Oceanogr*., **64**, 789-802, 2008.

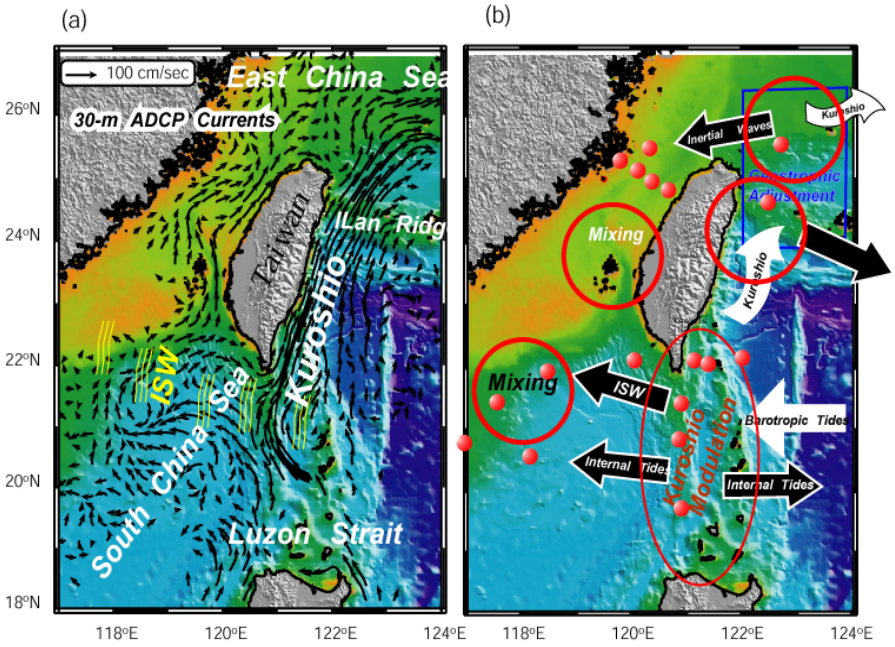

Figure 1: (a) Topography of western Pacific near Taiwan. Composite shipboard ADCP velocity at 30-m depth (figure adopted from Liang et al. 2003) shows Kuroshio crossing regions of strong topography in Luzon Strait and impinging on the continental shelf of the East China Sea northeast of Taiwan. (b) Potential small-scale processes in the region. Potential hot spots for generation of internal waves and turbulence mixing are red circled in (b). Red bullets mark positions of available mooring data for the present analysis.

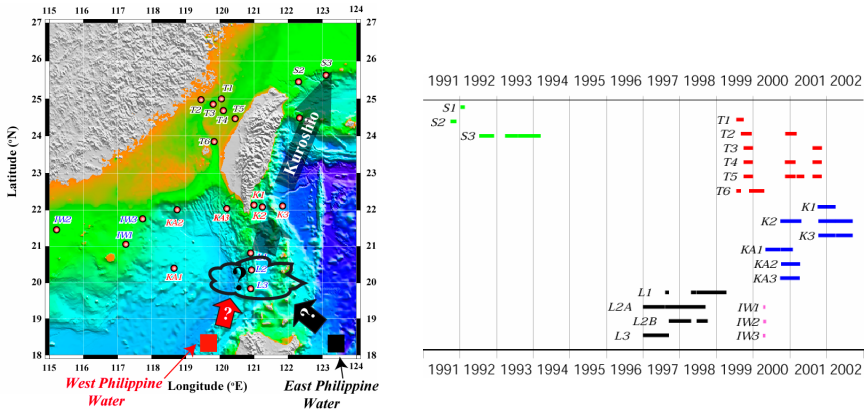

Figure 2: Positions (left panel) and periods (right panel) of moored ADCPs and current meters in East China Sea, Taiwan Strait, Kuroshio, Luzon Strait, and South China Sea. Stations of current meter and ADCP moorings are labeled. Red and black blocks represent the area where water masses are commonly defined as South China Sea water and Kuroshio water, respectively. We emphasize in our analysis that this definition is misleading and term them as west Philippine water and east Philippine water, respectively. In the main axis of the Kuroshio, e.g., station K2, the water mass is a mixture of these two water types.

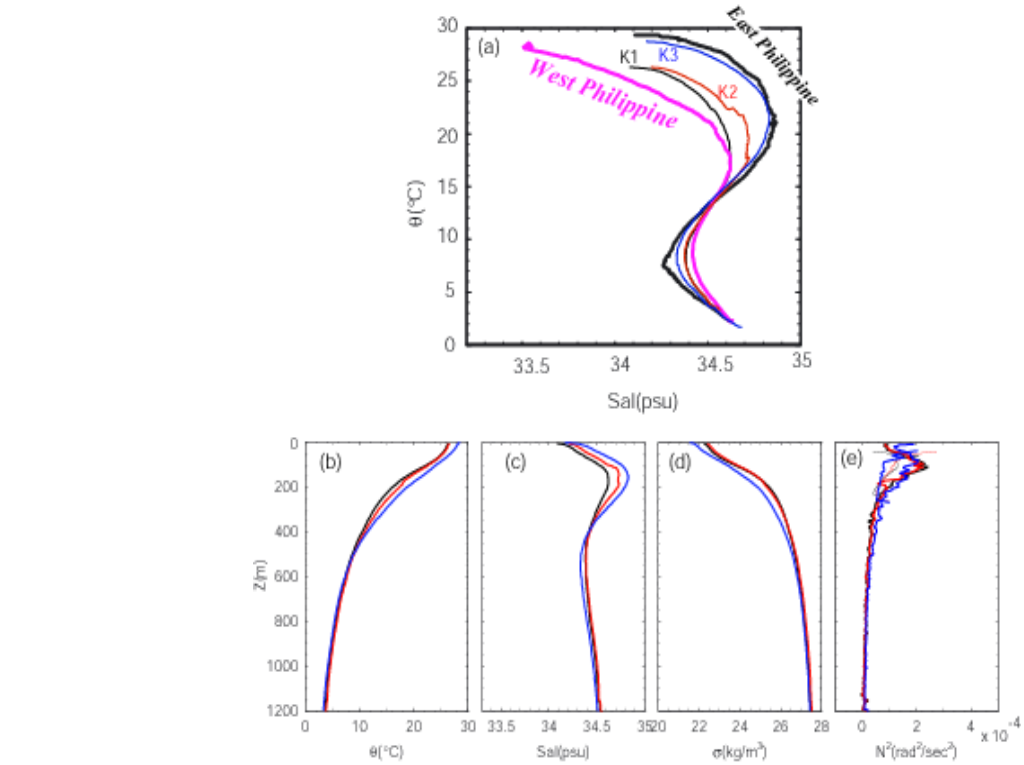

Figure 3: Water properties at three mooring positions, K1 (black), K2 (red), and K3 (blue). The panel (a) shows T-S properties of water masses at mooring stations, west Philippine water (magenta), and east Philippine water (thick black). Vertical profiles of potential temperature, salinity, potential density, and N^2 are shown in panels (b), (c), (d), and (e).Thin curves in panel (e) are total shear squared computed from mooring ADCP data.

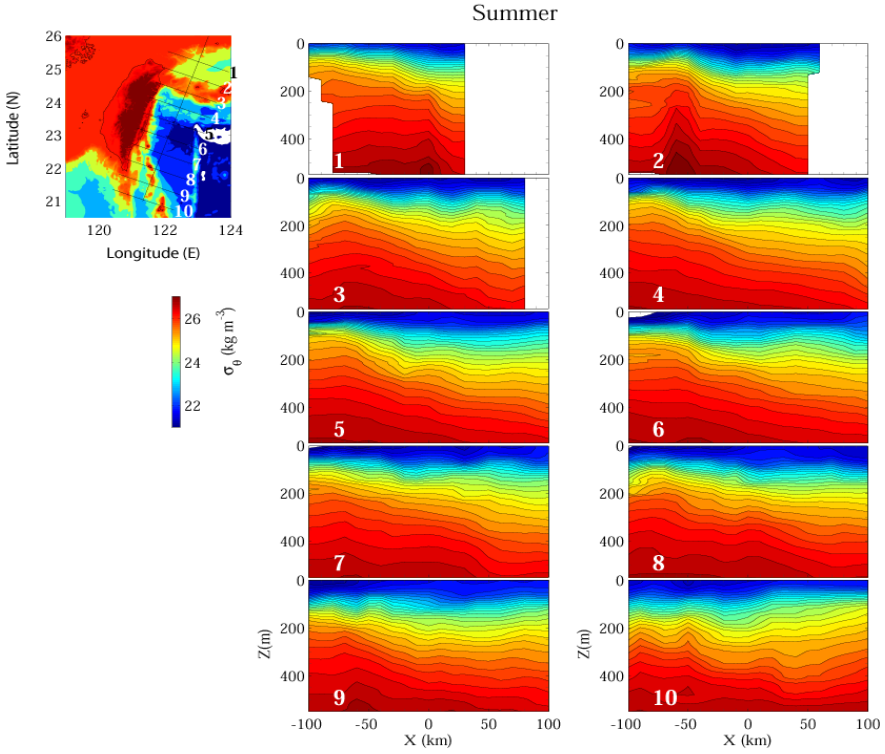

Figure 4: Average density fields in summer across the Kuroshio along the east coast of Taiwan constructed using historical CTD data.

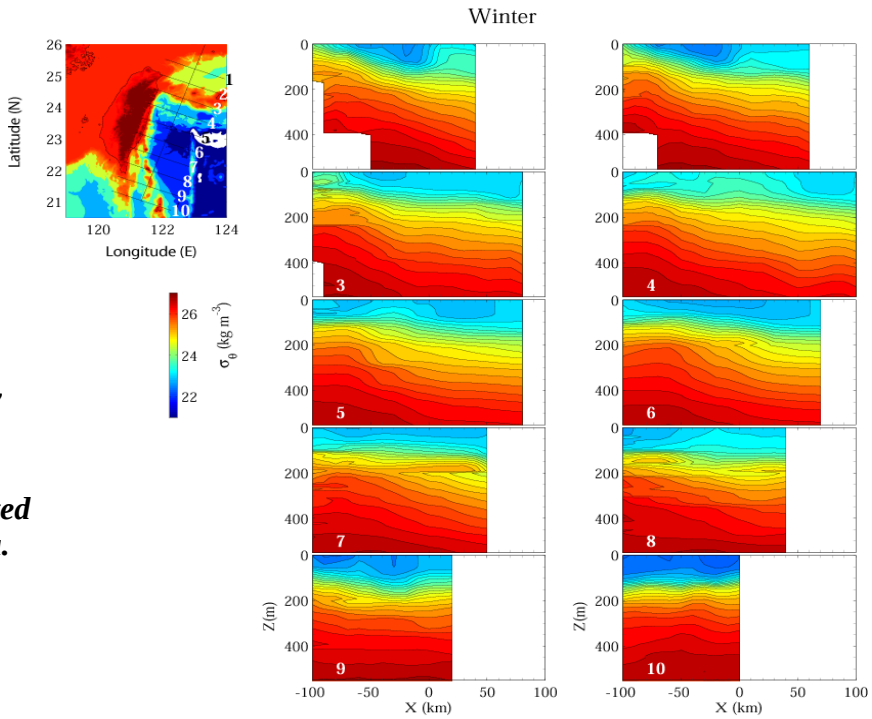

Figure 5: Average density fields in winter across the Kuroshio along the east coast of Taiwan constructed using historical CTD data.

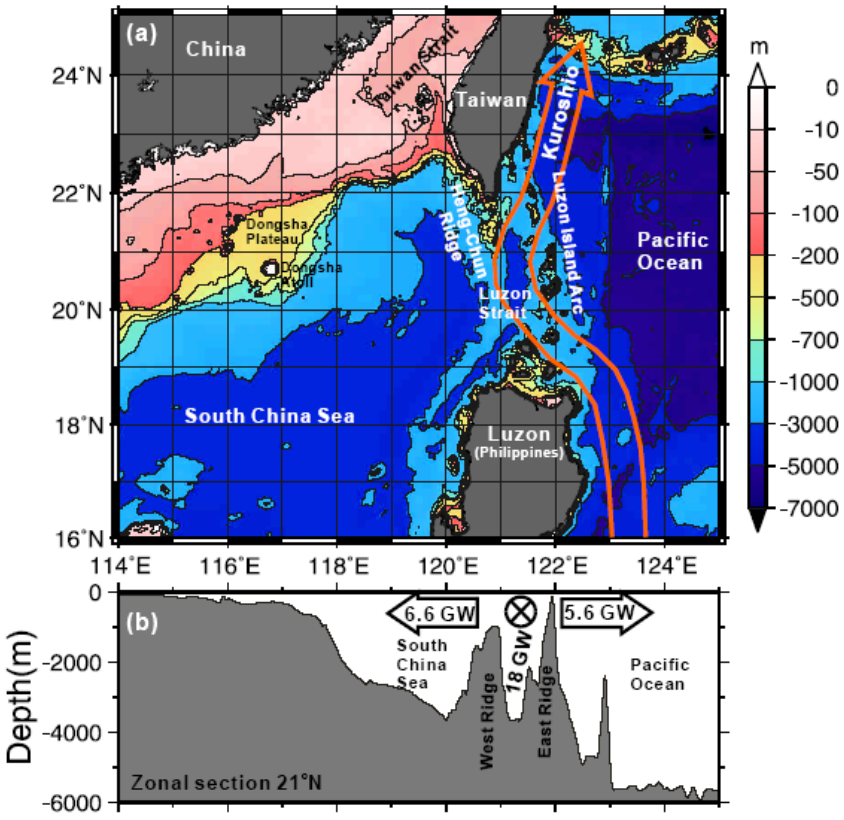

Figure 6: (a) Bathymetry in the northern South China Sea, northwest Pacific Ocean and Luzon Strait. (b) Topographic transect along 21^{o}N and main results of baroclinic tidal energy fluxes and dissipation. Arrows of 6.6 and 5.6 GW represent the spring-neap mean baroclinic energy fluxes that propagate into the South China Sea and the Pacific Ocean, respectively, from the Luzon Strait. About 18 GW of the baroclinic tide dissipation occurs in the Luzon Strait. ⊗ marks the Kuroshio.

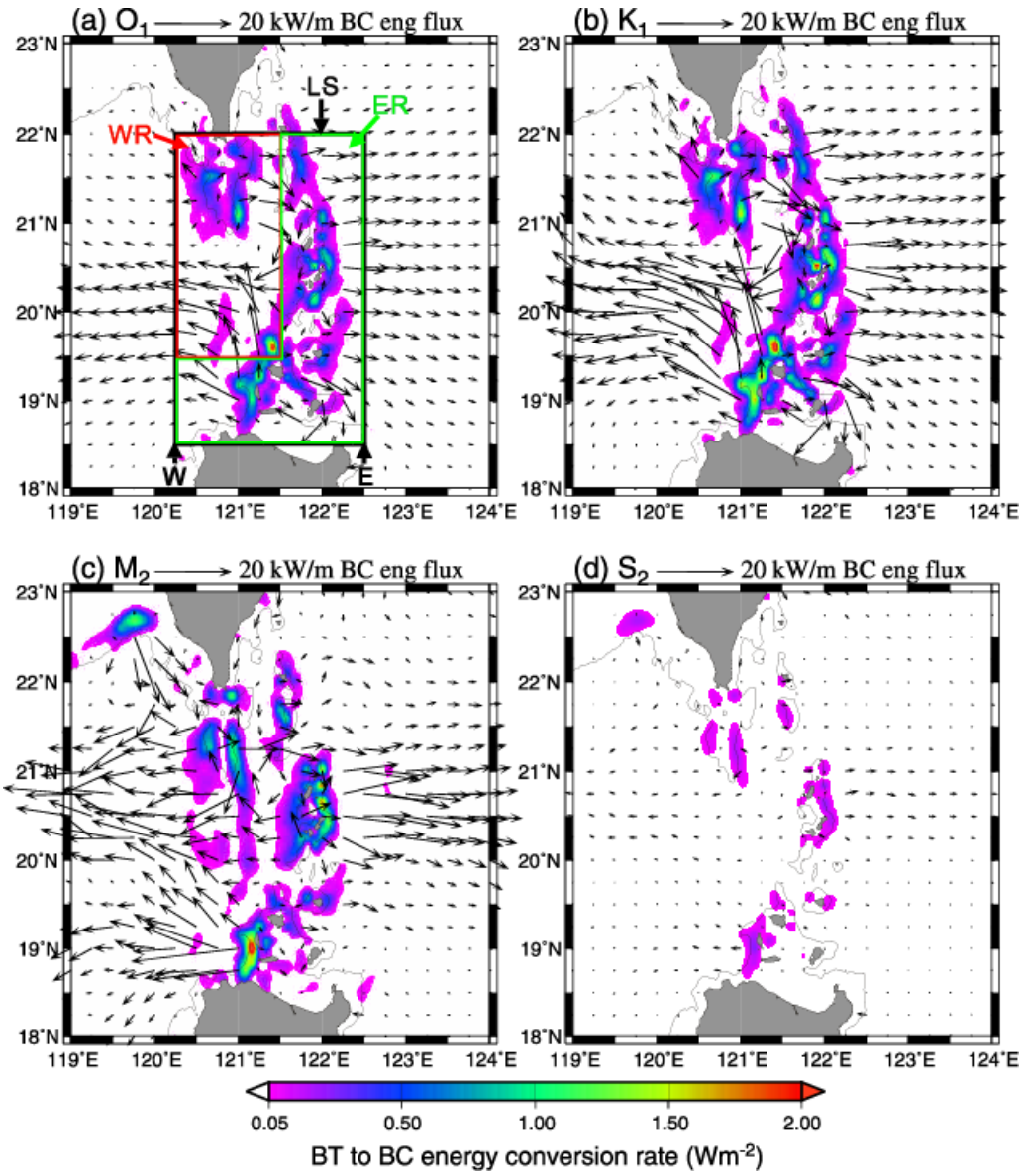

Figure 7: Spatial distribution of depth-integrated barotopic-to-baroclinic energy conversion rate (color shading) and baroclinic energy flux(vectors) for (a) O_1, (b) K1, (c) M_2, and (d) S_2 constitutents in summer. The black contour line represents the 1000-m isobath.

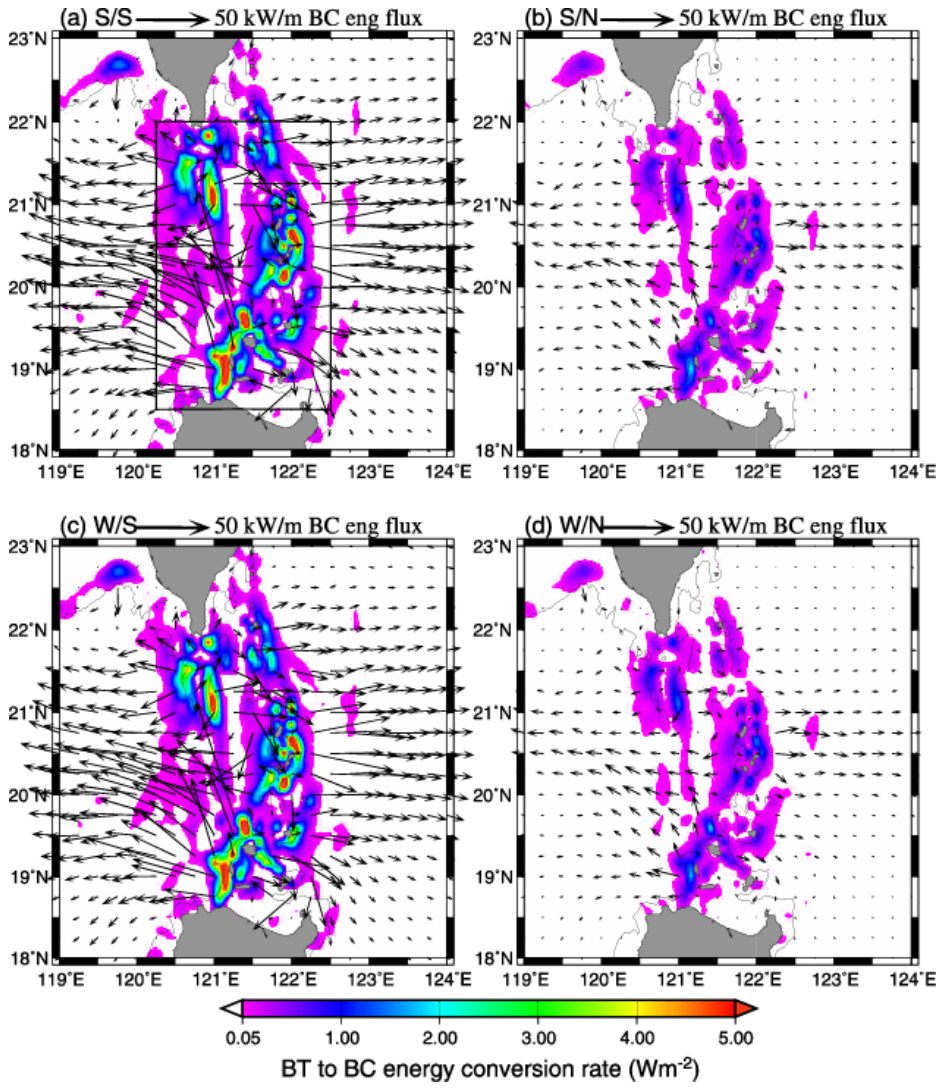

Figure 8: Spatial distribution of depth-integrated barotopic-to-baroclinic energy conversion rate (color shading) and baroclinic energy flux (vectors) for combined major tidal constituents O1, K1, M2, and S2 in (a) summer spring period, (b) summer neap period, (c) winter spring period, and (d) winter neap period. The black contour line represents the 1000-m isobath.